Special Issue Article

Journal of Intelligent Material Systems and Structures

Journal of Intelligent Material Systems and Structures
2015, Vol. 26(9) 1128–1137

DOI: 10.1177/1045389X15577643
jim.sagepub.com
SAGE

An experimental method to design piezoelectric energy harvesting skin using operating deflection shapes and its application for self-powered operation of a wireless sensor network

Hongjin Kim[1], Sowon Lee[2], Chulmin Cho[1], Jae Eun Kim[3], Byeng Dong Youn[1] and Yoon Young Kim[1]

Abstract
This work proposes a more practical way of designing the piezoelectric energy harvesting skin, which facilitates the application of the proposed idea to any practical engineering facilities with vibration. Unlike earlier studies to make use of analytical model for piezoelectric energy harvesting design, this work proposes an experimental method to design a piezoelectric energy harvesting skin using operating deflection shapes of a target mechanical system. This method is more practical in the sense that actual vibration of a target mechanical system can be characterized far better for the piezoelectric energy harvesting design. The key idea is to extract continuous in-plane normal strain values from discrete out-of-plane deformations of a target mechanical system. From multiple strain inflection lines, piezoelectric energy harvesting skin segments are designed to maximize a total power output. It is demonstrated that four piezoelectric energy harvesting skin segments designed by the proposed idea can generate sufficient power from the outdoor condensing unit of an air conditioning for self-powered operation of a wireless sensor network.

Keywords
Energy harvesting, operating deflection shape, strain inflection line, wireless sensor

Introduction

Energy harvesting from ambient sources has been recognized as a promising powering technology for portable or wireless electrical devices (Anton and Sodano, 2007; Hudak and Amatucci, 2008; Priya and Inman, 2009; Roundy and Wright, 2004). Among various types of energy sources and energy harvesting mechanisms, piezoelectric energy harvesting (PEH) from mechanical vibration has received much attention because of its promising power density, high energy conversion efficiency, and abundant presence around sensor locations (Cook-Chennault et al., 2008; Erturk and Inman, 2011; Roundy et al., 2003; Sodano et al., 2004).

PEH has been realized in various structural forms (Kim et al., 2004, 2005a, 2005b; Wang, 2007; Wang and Xu, 2007), one of which is a well-known simple cantilever type. In order to overcome the drawbacks of the cantilever-type PEH, a skin-type piezoelectric energy harvester was also introduced by Lee and Youn (2011a, 2011b). In the earlier works on the PEH skin design, a skin is formed with thin piezoelectric patches attached directly onto a vibrating shell structure, which can be found in various kinds of mechanical systems such as heating, ventilation, and air conditioning (HVAC) facilities; home appliances; vehicles; and so on. The structure is considered as a substrate for thin piezoelectric patches. Directly attached to a target mechanical system, a PEH skin does not require an additional fixture unlike a cantilevered PEH device.

[1]WCU Multiscale Design Division, School of Mechanical and Aerospace Engineering, Seoul National University, Seoul, Republic of Korea
[2]Hyundai Motors, Gyeonggi-do, Republic of Korea
[3]School of Mechanical and Automotive Engineering, Catholic University of Daegu, Gyeongsan-si, Republic of Korea

Corresponding author:
Yoon Young Kim, WCU Multiscale Design Division, School of Mechanical and Aerospace Engineering, Seoul National University, 1 Gwanak-ro, Gwanak-gu, Seoul, 151-744, Republic of Korea.
Email: yykim@snu.ac.kr

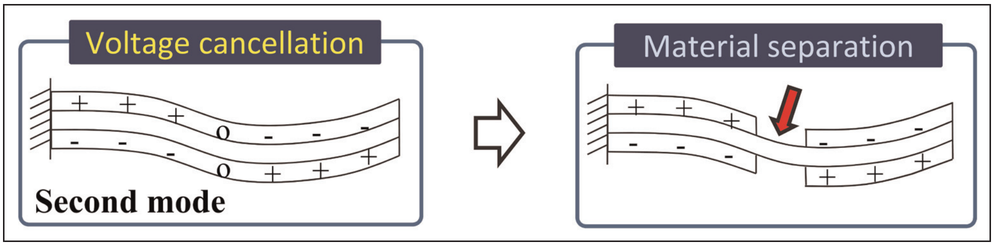

Figure 1. Phenomenon of voltage cancellation on a cantilever in the secondary vibration mode and a material separation idea to eliminate the cancellation.

The voltage cancellation effect (Erturk et al., 2009; Kim et al., 2005b; Lee et al., 2009; Rupp et al., 2009) should be taken into account for maximizing the harvested power. If a single piezoelectric patch experiences the voltage cancellation as shown in Figure 1, the generated power can be substantially reduced. Separation of one patch into multiple patches is thus inevitable for power maximization. So far, two methods (Erturk et al., 2009; Lee and Youn, 2011b) have been investigated to implement the patch separation lines along with (a) voltage phase changes and (b) in-plane normal strain sign changes.

Lee and Youn (2011b) analytically addressed a multimodal PEH skin design by considering multiple harmonic vibration modes. However, the analytical approach to the PEH skin design is limitedly applicable because it is extremely difficult to precisely model the vibration response of an actual mechanical system. In this work, instead of applying the finite element (FE) analysis, experimentally measured operating deflection shapes (ODSs) of a target mechanical system are employed to find strain inflection lines for the PEH skin design. Multiple inflection lines found at specific excitation frequencies are used for the final design of a PEH skin to enhance the energy harvesting capability. The proposed design methodology was demonstrated by applying to an outdoor condensing unit as a vibrating structure. The effectiveness of the study was experimentally verified by powering five wireless sensors (four accelerometers and one temperature sensor) with four PEH skin segments.

PEH skin design procedure based on ODS

Theoretical background of the strain inflection line

As mentioned, it is noted that a key step in the PEH skin design is to properly identify strain inflection lines so as to minimize unwanted power loss due to the voltage cancellation effect. In this work, the PEH skin can be segmented by the strain inflection lines identified using the in-plane normal strain distributions that are calculated from the ODS data of a target mechanical system. In general, a piezoelectric skin (0.127–0.267 mm) is much thinner than a vibrating substrate structure (1.0–3.0 mm). It is assumed to have a perfect bonding between the skin and the shell structure in this study. It is thus reasonable to say that the average strain distribution of the skin is similar to that of the substrate structure. Relying on rather an experimental approach than a simulation, it is nearly infeasible to identify strain inflection lines by output voltage phase (Lee and Youn, 2011b), which cannot be measured prior to the skin segmentation. A theoretical background on the identification of strain inflection lines based on in-plane normal strains is briefed in the following for clear understanding of the proposed experimental skin design (Erturk, 2011).

For a piezoelectric patch with an external load resistance (R_L), the integral form of Gauss's law for a dielectric material can be expressed as

$$\frac{\mathrm{d}}{\mathrm{d}t}\left(\int_A \mathbf{D}\cdot\mathbf{n}\mathrm{d}A\right) = \frac{v(t)}{R_L} \tag{1}$$

where $\mathbf{D}$ is the electric displacement vector, $\mathbf{n}$ is the unit outward normal vector, A is the electrode area of a piezoelectric patch, and $v(t)$ is the voltage across the external load resistance R_L.

For a thin piezoelectric patch undergoing the in-plane strains in the xy plane (see Figure 2), the electric displacement in the thickness direction is expressed as

$$D_3 = \bar{e}_{31}S_1 + \bar{e}_{32}S_2 + \bar{\varepsilon}^S_{33}E_3 = \bar{e}_{31}(S_1 + S_2) + \bar{\varepsilon}^S_{33}E_3 \tag{2}$$

where S_1 and S_2 are the in-plane normal strain components, E_3 is the electric field intensity in the thickness direction, $\bar{e}_{31}$ and $\bar{e}_{32}$ are the piezoelectric stress constants, and $\bar{\varepsilon}^S_{33}$ is the dielectric permittivity at constant strain. The over-bar denotes the reduced quantities resulting from neglecting the transverse shear and thickness stress components and considering the transversely isotropy of piezoelectric material such as lead zirconium titanate (PZT). The reduced piezoelectric stress constants and dielectric permittivity can be, respectively, obtained as

$$\bar{e}_{31} = \bar{e}_{32} = \frac{d_{31}}{s^E_{11} + s^E_{12}},\ \bar{\varepsilon}^S_{33} = \varepsilon^T_{33} - \frac{2d^2_{31}}{s^E_{11} + s^E_{12}} \tag{3}$$

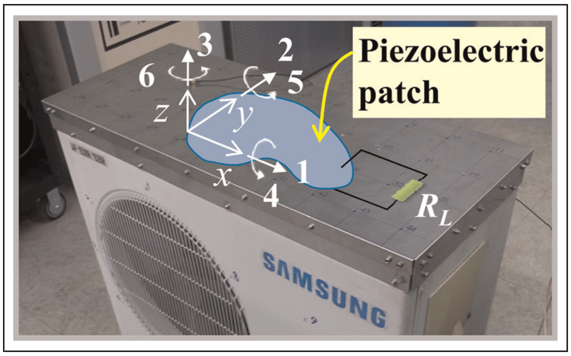

Figure 2. Schematic representation of a PEH skin, attached onto a structure undergoing two-dimensional surface strain fluctuations.

where s_{11}^E and s_{12}^E are the elastic compliances at constant electric field, d_{31} is the piezoelectric strain constant, and ε_{33}^T is the dielectric permittivity at constant stress.

For more useful form of equation (1), if the only nonzero electric displacement component shown in equation (2) is substituted into equation (1) and the electric field intensity is expressed in terms of the voltage across the external load resistance (R_L), equation (1) leads to

$$\frac{\mathrm{d}v(t)}{\mathrm{d}t} + \frac{v(t)}{R_L C_p} = \frac{\bar{e}_{31}}{C_p}\int_A \frac{\partial}{\partial t}[S_1(x,y,t) + S_2(x,y,t)]\mathrm{d}A \quad (4)$$

where $C_p = \bar{\varepsilon}_{33}^S A/h_p$ is the capacitance of a piezoelectric patch and h_p is the thickness of a piezoelectric patch. Therefore, the voltage response is obtained from equation (4) as follows

$$v(t) = \frac{\bar{e}_{31}}{C_p} e^{\frac{-t}{\tau}} \int e^{\frac{t}{\tau}} \left\{ \int_A \frac{\partial}{\partial t}[S_1(x,y,t) + S_2(x,y,t)]\mathrm{d}A \right\} \mathrm{d}t \quad (5)$$

From the equation above, it is obvious that the output voltage of a PEH skin is directly related to the sum of two in-plane normal strain components, which is invariant irrespective of measurement directions in the xy plane. In the proposed PEH skin design, therefore, the criterion to properly determine strain inflection lines is simply to identify the locations at which the sum of two in-plane normal strain components becomes zero, that is, $S_{sum} = S_1 + S_2 = 0$.

Design process based on ODS

Designing a PEH skin requires two in-plane normal strain components (S_{sum}) to locate the strain inflection lines. It is impossible to measure the in-plane normal strains over a large area. This work instead measures the out-of-plane deflection (i.e. the ODS) of a target mechanical system and then calculates the in-plane normal strain components using a mathematical relationship as follows:

Step 1. Select a target mechanical system and determine grid information (i.e. size, number of grid points, etc.) considering size of the target mechanical system and vibration mode.
Step 2. Measure ODS and determine frequency ranges of interest, having meaningful deflection shapes. Acquire the out-of-plane deflection data of the target mechanical system at the frequencies of interest.
Step 3. Represent the out-of-plane deflection data using polynomial curve fitting.
Step 4. Calculate the sum of the in-plane normal strain from the fitted out-of-plane deflection, using the following equation (see Stanbridge et al., 2002) as

$$S_{sum} = S_1 + S_2 = \frac{h}{2}\left(\frac{\partial^2 w}{\partial x^2} + \frac{\partial^2 w}{\partial y^2}\right) \quad (6)$$

where h and w represent the plate thickness and the out-of-plane deflection, respectively.
Step 5. Draw the strain distributions using the calculated in-plane normal strain values over the target surface and locate the zeroes of S_{sum} for the strain inflection lines.
Step 6. Determine the number of the strain inflection lines of which the harmonics are included in the frequency ranges of interest.

Target selection and vibration characterization

Target selection and modifications

The proposed design method enhances a practical aspect of the PEH skin, so that it can be applied to operating plant facilities. Prior to such a practical application, an in-lab facility was devised clearly to validate the proposed idea and realize potential challenges in a practical situation. Unlike most experimental validation works executed with an ideal structure and an electromagnetic shaker, this work employed the outdoor condensing unit of an air conditioner as a target mechanical system as shown in Figure 3(a). Given harmonic vibrations produced by a cooling fan inside (operating at 1170–1180 r/min), the outdoor condensing unit with a large top plate ($800 \times 300 \times 1$ mm^3) is very appropriate for the demonstration study of the PEH skin design.

After examining vibration characteristics of the top plate, it is found that the characteristics results were not reproducible. This was because of mixed and heavily random boundary conditions. While rigidly constrained by two side walls, the plate was loosely constrained by two other side walls and upheld at the center by an inner vertical supporter. Especially, the inner supporter was considered to be the main cause of this randomness since it was loosely upholding the top plate without any solid fixing. In addition, the maximum vibration on the top plate transmitted from a cooling fan inside was measured at the level of 0.1–0.2g (1g = 9.8 m/s^2). The level is relatively very low in comparison with that found in actual plant facilities, which is in the range of 2–3g (measured from a fan blower unit in the first power plant, Seoul National University).

Therefore, as shown in Figure 3(b), the outdoor condensing unit was modified to enhance the measurement reproducibility by minimizing the randomness in the boundary conditions. Also, to simulate the actual vibration level found in plant environments, a small mass of eccentricity is intentionally imposed on the outdoor condensing unit although the life of the unit would be reduced. The modification was thus done in threefold by (a) replacing the top plate having flat surface without any embossed region, (b) extending heights of the side walls so that the inner vertical supporter cannot interfere with the top plate, and (c) adding a mass of 20 g to one of the three blades in a cooling fan. In summary, the top plate becomes clamped along the sides only with increased vibration level through the modification.

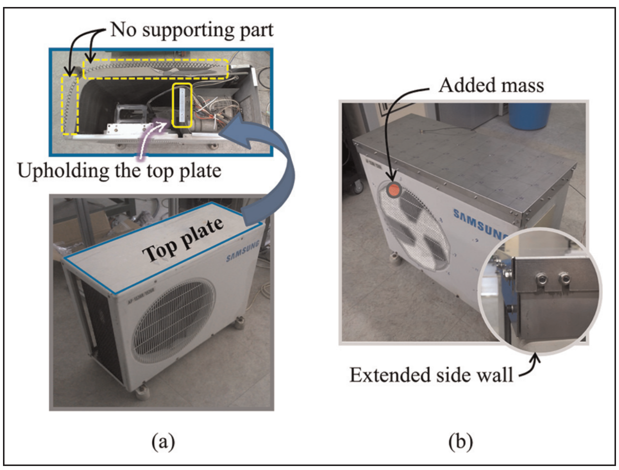

Figure 3. (a) Structure of the outdoor condensing unit with mixed and heavily random constraints of the top plate and (b) modification of the condensing unit with extended side walls and an added mass.

Vibration characterization

After the modifications, the vibration characteristics of the top plate was again measured and characterized. This characterization process, to be of great essence for a successful PEH skin design, employs two measurement techniques: modal testing and ODS characterization.

First, modal testing using an impact hammer (086C03; PCB Piezotronics, Inc.) and an accelerometer (type 4394; Brüel and Kjær) was performed to examine vibration characteristics of the top plate (Ewins, 2000) at 11×5 grid points. The result of the modal testing proves that the modified top plate has reproducible vibration characteristics. The first three mode shapes of the top plate are shown in Figure 4(a), and the corresponding resonance frequencies are found to be 32.7, 48.3, and 69.9 Hz, respectively. The resonance frequencies are very difficult to predict by simulation (such as

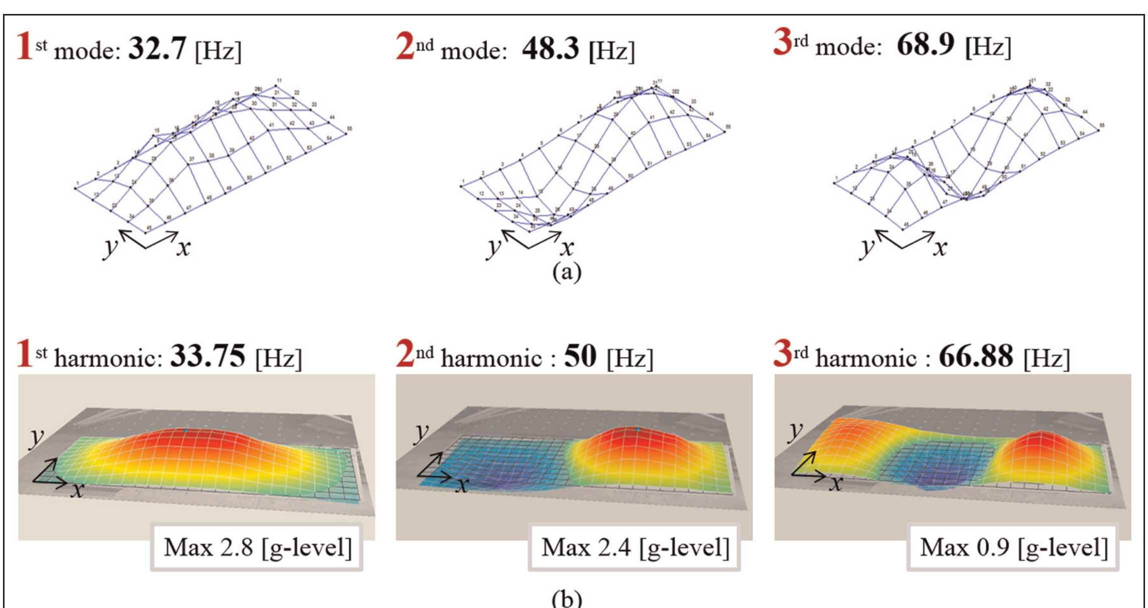

Figure 4. Identified vibration characteristics of the outdoor condensing unit's top plate: (a) mode shapes at the first three resonance frequencies and (b) three operating deflection shapes at frequencies of interest.

FE analysis) unless well-tuned boundary conditions are used. While the tuning itself poses much challenge, the simplified analysis with ideal fully clamped boundary conditions predicts the resonance frequencies of 97.7, 116.8, and 151.9 Hz, which are far off from the experimental results. This discrepancy highlights the importance of this experimental method because it is free from the prediction error inherent in simulation. Later, we found that the discrepancy is mainly caused by the unacknowledged modeling errors in boundary conditions and material modeling.

Then, the ODS characteristics of the top plate were examined to check a vibration response in the presence of actual excitation and select the frequencies of interest. Known as the driving frequency of 19–20 Hz induced by the fan rotation (1170–1180 r/min), the lowest peak frequency measured on the top plate was around 18 Hz prior to the modification but slightly lowered to 16–17 Hz after the modification. The eccentricity by the added mass has interfered with the fan rotation, resulting in a slightly lowered driving frequency. The ODS results are shown in Figure 4(b). In this work, a scanning laser vibrometer (PSV-400; Polytec GmbH) was used to measure the out-of-plane deflection of the top plate at 25×11 grid points to obtain the ODS. Three meaningful deflection shapes having large deformation were found at 33.8, 50.0, and 66.9 Hz, and the corresponding peak acceleration levels were measured as 2.8, 2.4, and 0.9g, respectively. It is noted that the measured three frequencies are near the harmonics of the first peak frequency (16-17 Hz), produced by the cooling fan rotation. Moreover, as compared in Figure 4, the ODS and modal testing results look very similar. This could occur because these three frequencies are near the resonance frequencies of the top plate by accident.

PEH skin design for the outdoor condensing unit

Using the measured ODS, a PEH skin can be designed by following the proposed design procedure. For a frequency of interest (e.g. 33.8 Hz), a total of 275 out-of-plane deflection data can be acquired from 25×11 grid points on the top plate shown in Figure 5(a).

Continuous out-of-plane deflection data are required to replicate the deformed shape of the top plate. The 275 data were employed for the polynomial curve fitting of the out-of-plane deflection. Before polynomial curve fitting, these data must be grouped in datasets along the grid lines. Along 11 grid lines in the x-direction, 11 datasets each having 25 values can be obtained. Similarly, 25 datasets each having 11 values are obtained in the y-direction. Then, MATLAB was

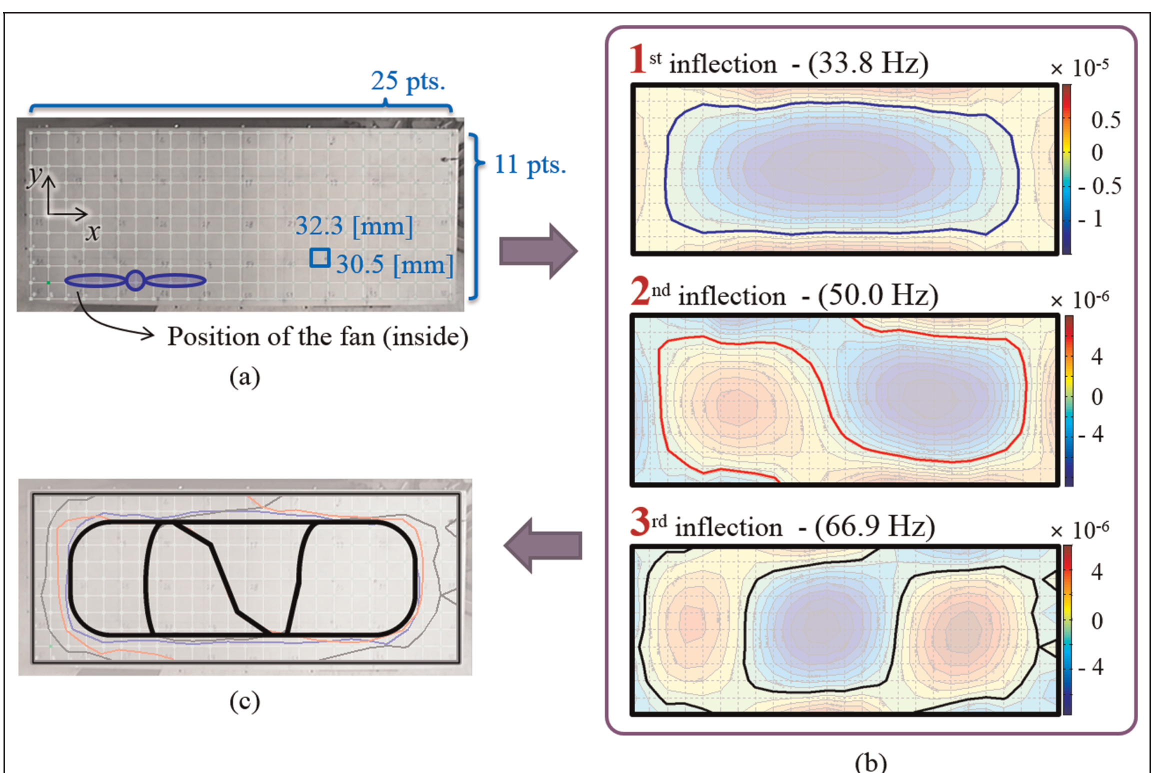

Figure 5. Schematic representation of the design procedures of the PEH skin: (a) grids on the top plate of the condensing unit to measure the ODS, (b) sum of in-plane strain distribution results and corresponding inflection lines at three frequencies of interest (i.e. 33.8, 50.0, and 66.9 Hz), and (c) the proposed design of the PEH skin by superposition of three strain inflection lines.

used to approximate the datasets with 4- to 8-order polynomials, which could best replicate the ODS of the top plate. The polynomials had the acceptable R^2 values of 0.990 and 0.970 in the x- and y-directions, respectively. As a result, the ODS of the top plate at the frequency of interest is expressed with 36 piecewise polynomials.

Given the continuous out-of-plane deflections from the ODS, the sum of in-plane normal strains S_{sum} can be calculated by applying equation (6). Figure 5(b) illustrates three strain inflection lines for three frequency values (33.8, 50.0, and 66.9 Hz) defined as the minimum of the absolute values of S_{sum}. Figure 5(c) shows the segmented design of the PEH skin. The design was obtained by superposing the strain inflection lines in the three harmonics while taking into account the manufacturability. In the superposition, a higher weight is applied to a lower frequency harmonic because the lower one produces much energy in general.

PEH skin fabrication and powering a wireless sensor network

Fabrication process of a PEH skin

The following steps are proposed to fabricate the PEH skin, and this process is also illustrated in Figure 6.

Step 1. Prepare a two-dimensional CAD file of the skin design in an actual size using a drawing software such as AutoCAD.

Step 2. Load the CAD file to a computer numerical control (CNC) laser cutter (M-300 Laser Platform; Universal Laser Systems, Inc.) and cut PZT sheets (PSI-5H4E; Piezo Systems, Inc.) using the laser cutter. Make sure the poling direction of the PZT sheets to be aligned consistently.

Step 3. Sketch the skin design on the top plate to locate the piezoelectric patches machined in Step 2.

Step 4. Attach the laser-machined PZT sheets to the top plate using a conductive epoxy (CW-2400; ITW Chemtronics). Make sure to prevent the overflow of the epoxy onto the PZT top surface, which causes an electric short.

Step 5. Check if any PZT sheet is electrically short or not. Redo Step 4 for the PZT sheets identified to be in electrically short state.

Step 6. Cure the epoxy for 6 hours at room temperature with a uniformly distributed weight of around 2 kg on the PZT sheets.

Step 7. Connect the PZT sheets in one PZT segment using an electric tape.

Validation of the proposed experimental method to design the PEH skin—self-powered operation of a wireless sensor network

The concept of a smart plant has been developed for optimal process, risk, and asset managements. This requires monitoring of many process, risk, and logistics parameters using advanced sensor technologies. It is thus expected to use wireless sensors extensively for remote and multipurpose monitoring. However, one of

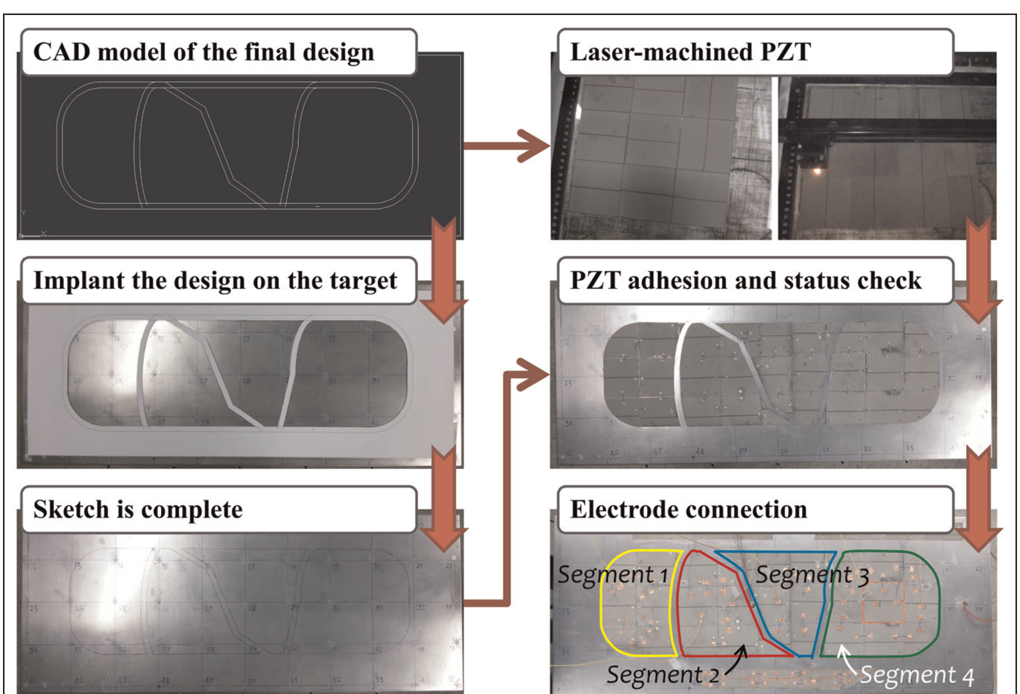

Figure 6. Proposed fabrication process of the PEH skin design.

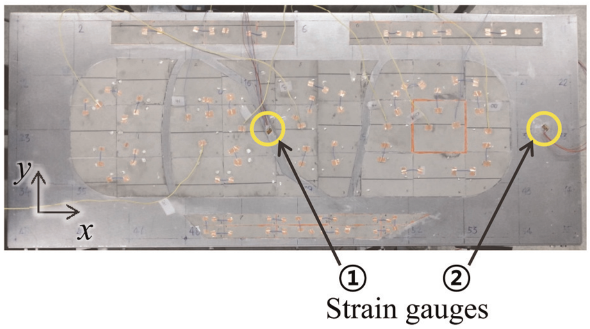

(unit: με)

	①: AT Inflection	②: NOT Inflection
x-dir	7	9
y-dir	6	75

Figure 7. Validation study and its result for the strain inflection lines of the proposed PEH skin design.

Table 1. Validation result for the voltage cancellation effect—voltage data harvested from different PEH segments (red and blue segments in Figure 8) divided by first and second inflection lines.

	V_{red}	V_{blue}	$V_{red} + V_{blue}$	$V_{red} - V_{blue}$
First inflection	4.28	4.94	3.34	5.16
Second inflection	4.09	4.53	2.38	5.50

Unit: V_{pp}.

the major concerns to use wireless sensors is a sustainable power source. We intended to propose the PEH skin as a sustainable power source to the wireless sensor network.

The objective of this section is to validate the effectiveness of the proposed experimental method in designing the PEH skin. The validation was done in three steps: (a) comparison of in-plane normal strain values on a strain inflection line with those on a noninflection line, (b) examination of the voltage cancellation effect between PZT segments divided by strain inflection lines, and (c) operation of a wireless sensor network using the power output of the PEH skin.

Validation 1—strain inflection lines. To validate the strain inflection lines, we attached two strain gauges at different locations; one on a strain inflection line and the other on a noninflection line (see Figure 7). The measured in-plane normal strains in the x- and y-directions, respectively, are also tabulated. The value of S_{sum} on the inflection line is far smaller than that on the noninflection line. It is valid to say that the strain inflection line is well identified with the negligibly small value of S_{sum}.

Validation 2—voltage cancellation effect. The voltage cancellation effect was examined by observing the output voltage phases of the PEH skin segments divided by the first and second strain inflection lines in the time domain, as shown in Figure 8(a) and (b), respectively. On the left graph of Figure 8(a), the solid red and dotted blue voltage curves were obtained from two PEH skin segments divided by the first strain inflection line. Although the two PEH skin segments are not in comparable size, out-of-phase tendency between the solid red and dotted blue voltage curves can be observed (see the dashed line box in Figure 8(a)). The voltage cancellation effect becomes clear when two PEH skin segments are electrically connected to form $V_{red} + V_{blue}$. For comparison, the voltage subtraction is mathematically performed to yield $V_{red} - V_{blue}$. The dotted black curve is the resultant voltage of $V_{red} + V_{blue}$ (see the right-hand side of Figure 8(a)). The solid green curve is the resultant voltage of $V_{red} - V_{blue}$. The green curve generates higher peak-to-peak values of output voltages, which are also tabulated in Table 1. It can be concluded that when designing a PEH skin, consideration of the voltage cancellation effect helps increase its power output.

For PEH skin segments divided by the second inflection line, the observations made above become more apparent. The solid red and dotted blue voltage curves obtained from two PEH skin segments are clearly out of phase from each other (see the left-hand side of Figure 8(b)). The voltage cancellation effect becomes more clear when $V_{red} + V_{blue}$ and $V_{red} - V_{blue}$ are compared. The peak-to-peak voltage results can be found in Table 1. From these observations, it is concluded that the PEH skin is well segmented across the inflection lines.

Validation 3—self-powered operation of a wireless sensor network. For the final verification of the proposed PEH skin design, five wireless sensors were employed. The detailed specifications of the wireless sensors can be found from the website of the manufacturer (AmbioSystems LLC, 2006). Each sensor was connected to the wireless platform (AmbioMote24; AmbioSystems LLC) of which the operating input voltage is informed to be between 5 and 80 V. To determine the lower limit of the operating voltage, a simple experiment was conducted using a function generator (33220A; Agilent), and the sensor was found to operate at over 2.3 V_{rms}.

The experimental setup to check sensor powering capability of the fabricate PEH skin is shown in Figure 9(a). Four three-dimensional acceleration

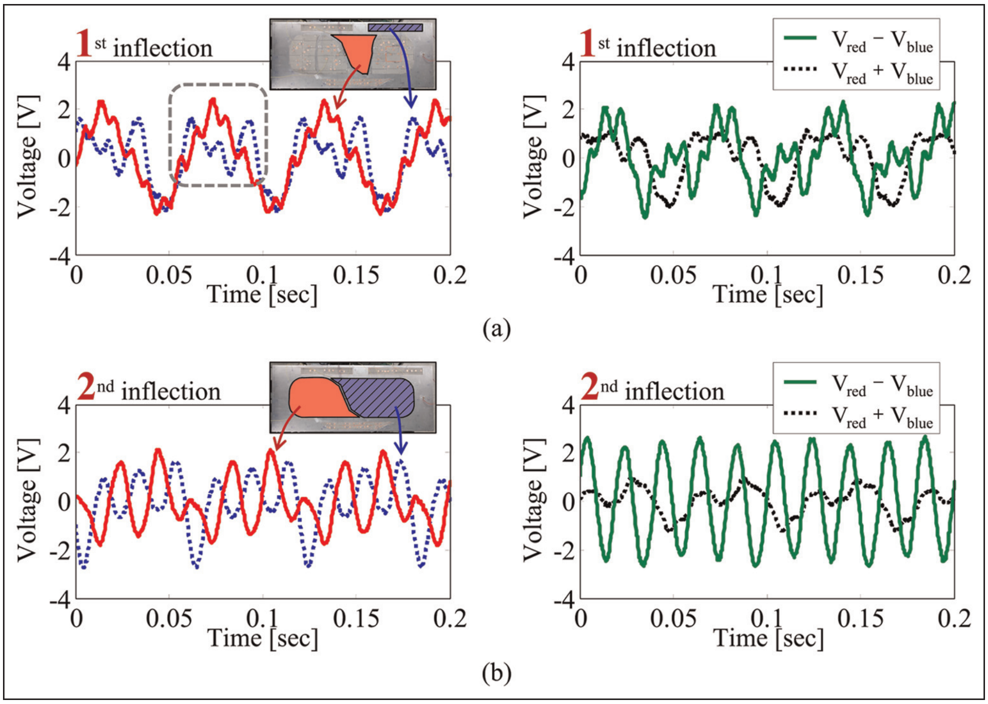

Figure 8. Validation study and its result for the voltage cancellation effect—voltage phases of the PEH segments divided by (a) first inflection line and (b) second inflection line.

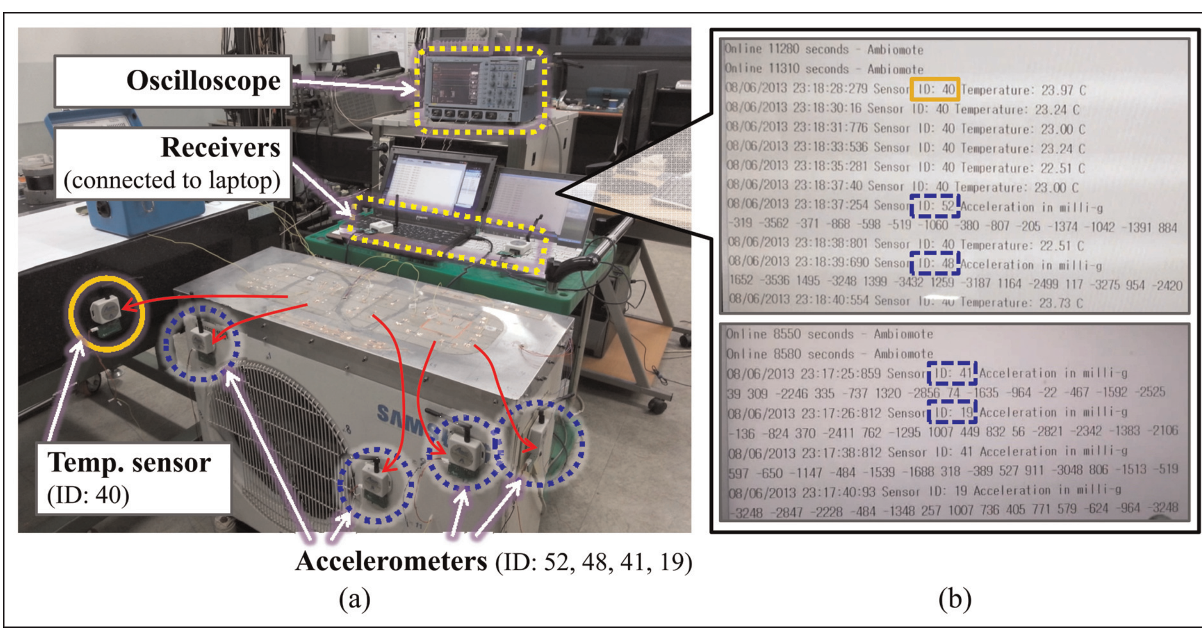

Figure 9. (a) Experimental setup for a self-powered operation of a wireless sensor network (four accelerometers and one temperature sensor) through its integration to the PEH skin and (b) real-time monitored sensory data from self-powered wireless sensor network.

sensors and one analog temperature sensor were directly connected to the PEH skin, and the wireless platforms were used to transmit sensor signals to a laptop computer. In addition, two receivers, each of which is connected to a different laptop, were used because one receiver could treat up to four sensor signals. When the outdoor condensing unit was in operation and each output power from the arbitrarily chosen four PEH skin segments was provided, it was observed that all five sensor signals were successfully transmitted to two laptops. The screenshots of two laptops are shown in Figure 9(b). The sensor signal from the temperature

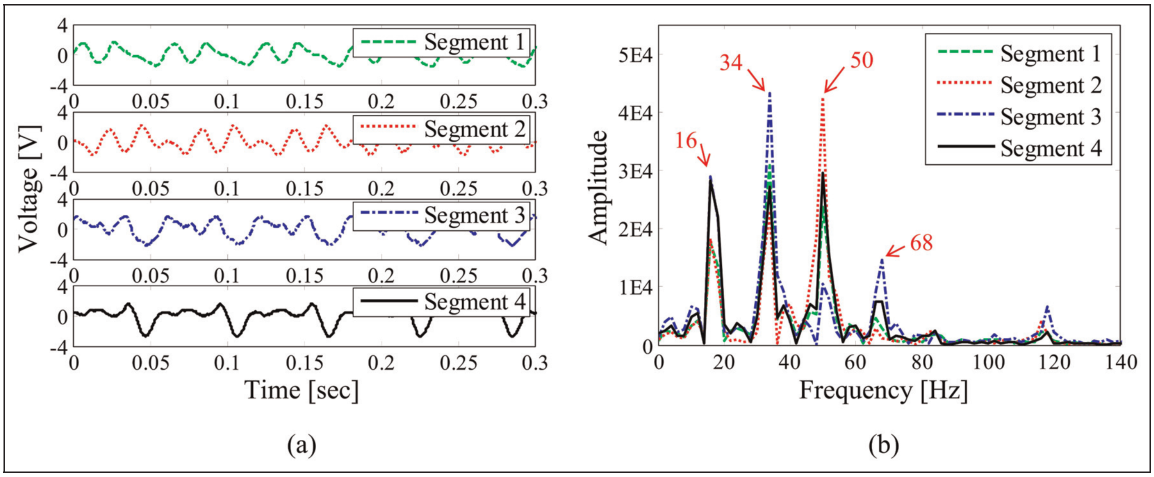

Figure 10. (a) Output voltage histories harvested from four PEH skin segments and (b) the fast Fourier transform result of the voltage signals.

sensor is highlighted with the orange solid lined box, while the blue dashed line boxes indicate the acceleration sensor signals.

An oscilloscope (LT354M; LeCroy) was also used to observe the output voltage in real time. Output voltage signals from the four PEH skin segments are shown in Figure 10(a) and their Fourier transformed pairs are shown in Figure 10(b). Output voltage from each PEH skin segment was measured as 4–5 V_{pp}. Four frequency peaks in Figure 10(b) and the ODS results in Figure 4(b) also confirm the consistency of the experiments.

Conclusion

This work proposes a practical method to design the PEH skin based on experimentally measured ODSs. The key idea is to replicate out-of-plane deformations of a target mechanical system using polynomial curve fitting and then calculate continuous in-plane normal strain values to find strain inflection lines. For final design of the PEH skin, multiple inflection lines found at specific excitation frequencies are used to enhance its energy harvesting capability. The proposed design procedure was applied to design a PEH skin for an outdoor condensing unit. This method is advantageous in many aspects against an analytical method: (a) free from unacknowledged modeling errors and (b) readily applicable to existing engineering facilities with vibration. The fabrication process was proposed, and the performance of the PEH skin was experimentally validated. The validation was conducted in three steps. First, the in-plane normal strain values on a strain inflection line were measured and compared with those on a noninflection line. The value of S_{sum} on the inflection line was turned out to be far smaller than that on the noninflection line, verifying the location of strain inflection line. Second, apparent voltage cancellation effect was examined between PEH skin segments divided by strain inflection lines, proving that the PEH skin is well segmented across the inflection line. Finally, the fabricated PEH skin is applied to operate a wireless sensor network, which is the most common but a still challenging application of the energy harvesting. The PEH skin could supply enough power to operate the wireless sensor network consisting of five wireless sensors.

The proposed PEH skin design procedure can be applied to various engineering facilities with vibration. However, in this study, the brittle material property of the PZT limited the PEH skin design to a flat area. To design a PEH skin for an actual plant facility, selection of piezoelectric materials having more flexibility could be more desirable. In the near future, we plan to design a PEH skin for an actual plant facility such as a fan blower unit. The generated power from the PEH skin will be supplied to operate wireless sensors for structural health monitoring of the facility.

Declaration of conflicting interests

The authors declared no potential conflicts of interest with respect to the research, authorship, and/or publication of this article.

Funding

This work was supported by the POSCO Grant (no. 2012Z048) and also supported by Basic Science Research Program (nos. 2014-021950 and 2013-055323) through the National Research Foundation of Korea (NRF) funded by the Ministry of Education, Science and Technology.

References

AmbioSystems LLC (2006) Product details of sensors for use with AmbioMote products. Available at: http://www.ambiosystems.com (accessed 13 April 2014).

Anton SR and Sodano HA (2007) A review of power harvesting using piezoelectric materials (2003–2006). *Smart Materials and Structures* 16: R1–R21.

Cook-Chennault KA, Thambi N and Sastry AM (2008) Powering MEMS portable devices—a review of non-regenerative and regenerative power supply systems with emphasis on piezoelectric energy harvesting systems. *Smart Materials and Structures* 17: 043001.

Erturk A (2011) Piezoelectric energy harvesting for civil infrastructure system applications: moving loads and surface strain fluctuations. *Journal of Intelligent Material Systems and Structures* 22: 1959–1973.

Erturk A and Inman DJ (2011) *Piezoelectric Energy Harvesting*. Chichester: John Wiley & Sons, Ltd.

Erturk A, Tarazaga PA, Farmer JR, et al. (2009) Effect of strain nodes and electrode configuration on piezoelectric energy harvesting from cantilevered beams. *Journal of Vibration and Acoustics* 131: 011010.

Ewins DJ (2000) *Modal Testing: Theory, Practice and Application*. 2nd ed. Baldock: Research Studies Press Ltd.

Hudak NS and Amatucci GG (2008) Small-scale energy harvesting through thermoelectric, vibration, and radiofrequency power conversion. *Applied Physics Letters* 103: 101301.

Kim HW, Batra A, Priya S, et al. (2004) Energy harvesting using a piezoelectric "Cymbal" transducer in dynamic environment. *Japanese Journal of Applied Physics* 43: 6178–6183.

Kim S, Clark WW and Wang Q (2005a) Piezoelectric energy harvesting with a clamped circular plate: analysis. *Journal of Intelligent Material Systems and Structures* 16: 847–854.

Kim S, Clark WW and Wang Q (2005b) Piezoelectric energy harvesting with a clamped circular plate: experimental study. *Journal of Intelligent Material Systems and Structures* 16: 855–863.

Lee S and Youn BD (2011a) A design and experimental verification methodology for an energy harvester skin structure. *Smart Materials and Structures* 20: 057001.

Lee S and Youn BD (2011b) A new piezoelectric energy harvesting design concept: multimodal energy harvesting skin. *IEEE Transactions on Ultrasonics, Ferroelectrics, and Frequency Control* 58: 629–645.

Lee S, Youn BD and Jung BC (2009) Robust segment-type energy harvester and its application to a wireless sensor. *Smart Materials and Structures* 18: 095021.

Priya S and Inman DJ (2009) *Energy Harvesting Technologies*. New York: Springer.

Roundy S and Wright PK (2004) A piezoelectric vibration based generator for wireless electronics. *Smart Materials and Structures* 13: 1131–1142.

Roundy S, Wright PK and Rabaey J (2003) A study of low level vibrations as a power source for wireless sensor nodes. *Computer Communications* 26: 1131–1144.

Rupp CJ, Evgrafov A, Maute K, et al. (2009) Design of piezoelectric energy harvesting systems: a topology optimization approach based on multilayer plates and shells. *Journal of Intelligent Material Systems and Structures* 20: 1923–1939.

Sodano HA, Inman DJ and Park G (2004) A review of power harvesting from vibration using piezoelectric materials. *Shock and Vibration Digest* 36: 197–205.

Stanbridge AB, Martarelli M and Ewins DJ (2002) Measuring strain response mode shapes with a continuous-scan LDV. *Shock and Vibration* 9: 19–27.

Wang S (2007) Energy harvesting with piezoelectric drum transducer. *Applied Physics Letters* 90: 113506.

Wang Z and Xu Y (2007) Vibration energy harvesting device based on air-spaced piezoelectric cantilevers. *Applied Physics Letters* 90: 263512.

Yoon H and Youn BD (2014) Stochastic quantification of the electric power generated by a piezoelectric energy harvester using a time–frequency analysis under non-stationary random vibrations. *Smart Materials and Structures* 23: 045035.